Appl. Phys. B 72, 591–597 (2001) / Digital Object Identifier (DOI) 10.1007/s003400100542

Applied Physics B
Lasers
and Optics

EUV and fast ion emission from cryogenic liquid jet target laser-generated plasma

M. Wieland[1,*,**], **T. Wilhein**[1,**], **M. Faubel**[2], **Ch. Ellert**[3,***], **M. Schmidt**[3], **O. Sublemontier**[3]

[1] Institut für Röntgenphysik, Universität Göttingen, Geiststr. 11, 37073 Göttingen, Germany
[2] Max-Planck-Institut für Strömungsforschung, Bunsenstr. 10, 37073 Göttingen, Germany
[3] CEA Saclay, DRECAM/SPAM, 91191 Gif sur Yvette, France

Received: 21 August 2000/Revised version: 20 December 2000/Published online: 22 March 2001 –

Abstract. A liquid jet of either nitrogen or argon of 20 μm diameter was exposed to intense laser fields with pulse durations between 70 fs and 250 ps, leading to intensities of 10^{16} W cm^{-2} and 10^{13} W cm^{-2}, respectively. The emission of extreme UV light and soft X-rays shows the characteristic lines of hydrogen-like nitrogen and carbon-like argon. For nitrogen the emitted photon flux at 250 ps was about two orders of magnitude higher than for 70 fs pulses. A weak dependence on the laser polarization with respect to the liquid jet axis was found. The kinetic energy of the emitted ions easily exceeded 100 keV for nitrogen and 200 keV for argon for a pulse duration close to 2 ps.

PACS: 33.80.Wz; 52.50.Jm; 29.25.Ni

Studies of X-ray and extreme ultra-violet (EUV) emission from laser-generated plasmas are of fundamental interest and lead simultaneously to promising applications. Of particular interest is the so-called water window between 2.4 nm and 4.4 nm, the wavelength range used for X-ray microscopy [1]. In addition, longer wavelengths between 10 nm and 20 nm are relevant for next-generation lithography which may enable structure size generation below 70 nm [2]. While solid targets have been studied for quite some time now (see [3] and references therein), clusters [4, 5] and liquid jets [6] only recently were recognized as targets of great interest. In this article we focus on continuous cryogenic liquid jet targets which have been scarcely studied so far.

Several parameters permit optimization of the soft X-ray and EUV emission. For example, the laser pulse duration critically affects the conversion efficiency of the laser energy because at constant focussing conditions it determines both the laser intensity and the duration of the laser–plasma interaction. Secondly, the atomic properties of the target material have two counteracting effects on the conversion efficiency. On the one hand, the heavier the atom the more emission lines of the ion are available for fine tuning of the emission, but less flux will be found in one particular line. On the other hand, the efficiency of the electron ion collisional heating by inverse bremsstrahlung, which is often the main heating mechanism in laser-generated plasmas from solid targets, increases with the average ionic charge state Z [3]. Thirdly, one could suspect an influence of the laser polarization relative to the liquid jet because both alternative non-collisional absorption mechanisms, e.g., resonant absorption [7] and "vacuum heating" [8, 9], show a strong dependence on the laser polarization. Eventually, while increasing the EUV emission yield, it is important to limit the debris emission from the plasma target in order to avoid damage of sensitive optical components, which could lead to a severe restriction for the application of laser-generated plasma light sources.

In the present work we address the following issues experimentally: the dependence of the EUV emission yield on (a) the laser pulse duration, (b) the target material and (c) the orientation of the laser polarization relative to the axis of the liquid jet and (d) the analysis of the kinetic energy of the ionic debris emitted from the expanding laser-generated plasma. Most high-intensity EUV sources based on a laser-generated plasma from high density gaseous or liquid targets operate in an environment of typically 10^{-3} mbar or higher. At such pressures the residual gas density is sufficiently high that it leads to a significant deceleration of the emitted ions due to collisions with the residual gas molecules. For this reason, kinetic energy distributions have never been reported before to our knowledge.

In the following, we first give a short description of the experimental setup, which includes the liquid jet production, the laser source, the EUV spectrograph and the ion detector. Then we present the EUV spectra and compare their characteristics with those obtained with other types of laser targets, e.g., cluster targets, or with other types of laser sources.

*Corresponding author.
(Fax: +49-2642/932-399, E-mail: wieland@rheinahrcampus.de)
**_Present address:_ University of Applied Sciences, Südallee 2, 53424 Remagen, Germany
***_Present address:_ TiNOX GmbH, Schwere-Reiterstr. 35/2b, 80797 München, Germany

1 Experimental setup

The major components of the experiment, sketched in Fig. 1, are (a) the cryostat for the production of liquid jets of the Max-Planck-Institut für Strömungsforschung and the University of Göttingen [10], (b) the intense laser facility LUCA of the DRECAM service at the CEA Saclay [11], (c) the EUV spectrograph and (d) the kinetic energy detector for the ions.

(a) The mechanical components of the liquid jet setup are similar to those described earlier in [6]. Briefly, the target material (N_2 or Ar) is cooled and liquefied in a cryostat filled with liquid nitrogen. The temperature in the cryostat can be varied within a limited range by controlling the vapor pressure of the liquid nitrogen reservoir. Typical operation values used are 2200 mbar (corresponding to ≈ 84 K) and 200 mbar (≈ 64 K) for argon and nitrogen, respectively. The possibility to vary the liquids temperature in the cryostat is necessary to obtain optimal thermodynamic conditions for the formation of a laminar argon or nitrogen flow, especially in the case of argon, for which extensive preparatory studies have been performed beforehand [10]. Thus, stable operation of a liquid argon jet was achieved for the first time. A stainless steel sintered filter with 0.5 μm pores removes particles and frozen gas impurities in order to avoid clogging of the nozzle before the liquid passes through a 20 μm circular orifice (platinum nozzle originally used in electron microscopy) into the main vacuum chamber. The backing pressure of the liquid jet varied between 20 and 40 bar. The vapor pressure within the vapor cloud that surrounds the liquid jet reaches 688 mbar (516 Torr) at the surface of liquid argon near its melting point at 83.80 K. The minimum vapor pressure for liquid nitrogen is 113 mbar (85 Torr) close to its triple point at 63.15 K. Thus, the liquid jet is surrounded by a thin gas layer with decreasing density, proportional to the reciprocal of radial distance. During jet operation a pressure of about 10^{-3} mbar was maintained with two 1000 l s^{-1} turbo drag pumps. The jet, which has a negligible divergence angle, was dumped after about 3 cm of free flight into a differential pumping stage. The latter was pumped by a roots blower with a pumping speed of 450 m^3/h, which was sufficient to keep the jet-dump below 1 mbar. Thus the largest fraction of the liquid jet target material was removed from the main chamber. Therefore, the pressure of this chamber was essentially due to evaporation from the liquid jet surface. Calculations based on a simple model for the evaporation process estimate the evaporated fraction to be around 20% of the jet material, depending on the jet diameter [10].

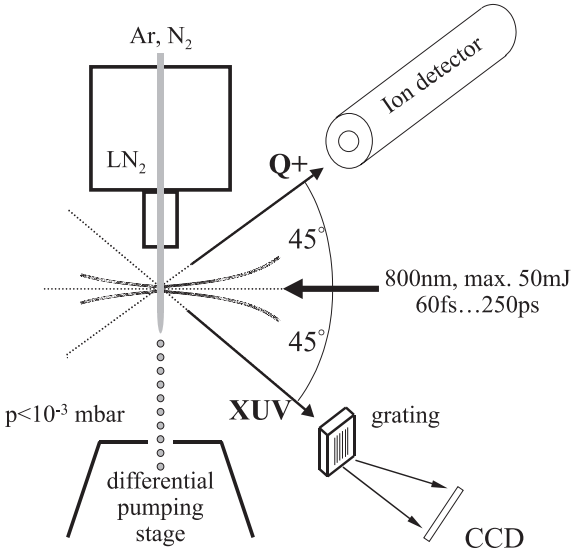

Fig. 1. The experimental setup consists of the liquid jet, the EUV spectrograph, the free flight kinetic energy spectrometer and the pulsed intense laser operating at 800 nm. The liquid jet and laser beam cross perpendicularly, whereas the spectrograph and the TOF axis are symmetrically positioned 45° right and left of the incoming laser

(b) The 800 nm laser system consists of a Ti:sapphire oscillator, amplified by one regenerative and two additional multi-pass amplifiers to 100 mJ. Half of this pulse energy has been at our disposal for the uncompressed 250 ps pulses. Passing through a grating compressor reduces the available power to 35 mJ for the experiments with a pulse duration between 70 fs and 2.5 ps. A half-wave plate followed by a polarizer allowed us to continuously vary the laser intensity without changing either the focusing conditions or the pulse length. By means of an additional half-wave plate the laser polarization could be rotated from parallel to perpendicular with respect to the liquid jet. The laser beam of 40 mm diameter was focused by a plano-convex $f = 500$ mm lens (focus size ≈ 40 μm) into the vacuum chamber onto the liquid jet typically 5 mm away from the nozzle within the contiguous part of the jet in order to obtain stable plasma formation. For the longest laser pulse duration of 250 ps this leads to an intensity of up to 10^{13} W cm^{-2}, while for 70 fs pulses about 10^{16} W cm^{-2} is applied onto the target.

(c) The slit-grating spectrograph for recording the EUV spectra is described in detail elsewhere [12]. It employs a free-standing transmission grating with 10 000 lines mm^{-1} and a total width of 120 μm. The grating material is gold on a silicon substrate. The grating was positioned at a distance of 59 cm away from the laser focus. Low-energy radiation and stray light from the laser was blocked by various filters, made of Al (≈ 220 nm), Sn (≈ 200 nm) or a combination of Si and Zr, each of 200 nm thickness. The filter transmission curves were obtained from [13]. The 1 mm height of the grating and a rectangular entrance slit of 50 μm width in front of the grating led to a collected solid angle of 1.4×10^{-7} sr for the spectrograph. The distance from the grating to the EUV-sensitive CCD camera was 41 cm. The described arrangement results in a spectral resolution of $\Delta\lambda \approx 0.024$ nm, assuming the size of the EUV source is 20 μm [12]. The number of analog–digital units (in the following counts) registered by the CCD varied between 2 and 1.4 counts per photon in the wavelength range from 15 nm to 20 nm, and between 12 and 5 counts per photon at 2 nm to 4 nm [14]. These values and the known grating efficiency, which was measured using synchrotron radiation and the calculated filter transmission, allow for absolute calibration of the recorded spectra and were taken into account in the vertical scale of Figs. 2 to 4. The accuracy of the obtained data is estimated to be better than 50%.

(d) The kinetic energy of the ions was measured by the time-of-flight method. However, at the elevated pressure in the main chamber during the liquid jet operation, the ion free path is on the order of several tens of centimeters only, as predicted by a hard spheres atom scattering model. In order to avoid strong alterations of the ion kinetic energy distribution due to collisional energy losses, we proceeded as

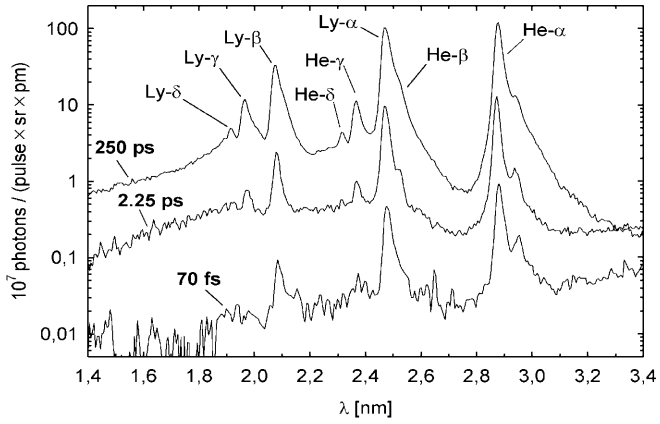

Fig. 2. EUV emission in the water window from the liquid nitrogen jet for different pulse lengths. The well-known Ly and He series of nitrogen are clearly visible. The spectra were recorded using an Al filter of 220 nm thickness in front of the grating; the pulse energy was 25 mJ

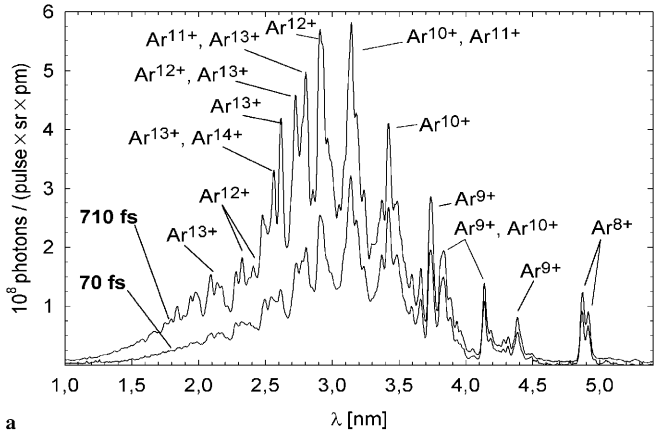

a

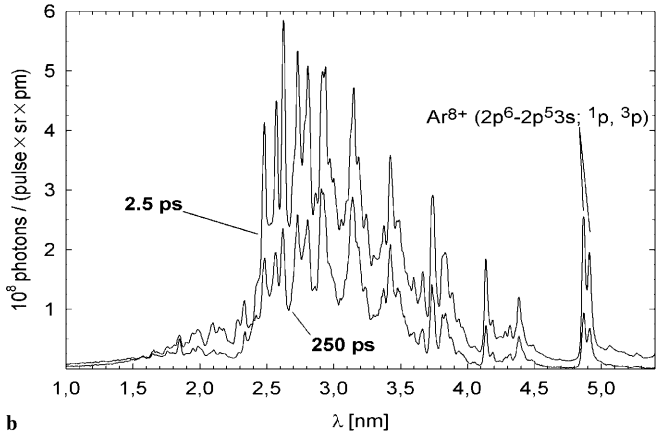

b

Fig. 3. a,b EUV emission in the water window from the liquid argon jet for different pulse lengths: **a** 70 fs and 710 fs; **b** 2.5 ps and 250 ps. The spectrum for a pulse duration of 2.5 ps was recorded with a Sn filter of 200 nm thickness, the others with an Al filter of 220 nm thickness. The laser pulse energy was 50 mJ at 250 ps and 30 mJ for the shorter pulses

follows: At about 10 cm from the interaction region we positioned a 1 mm entrance hole of an independently pumped flight tube of 10 mm diameter and 20 cm length. The differentially pumped region of the ion spectrometer with a free flight section of 50 cm total length could be kept at a pressure of better than 10^{-6} mbar during jet operation. Since the mass of the detected ions is known, this simple device is sufficient to measure the kinetic energies independent of the ionic charge state. The measured kinetic energy distribution of the ions represents a lower limit of the real distribution, which emerges from the laser–plasma interaction. By applying a post-acceleration voltage in front of the electron multiplier detector it was possible in some special cases at low initial kinetic energy to separate different charge states of the ions. Likewise, applying a negative bias voltage at the entrance grid of the TOF detector leads to verification of the fact that the incoming particles were indeed positively charged and that a negligible fraction of the signal was due to electrons.

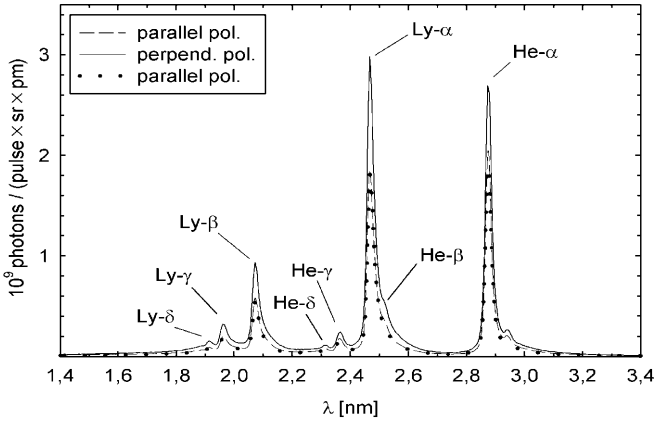

Fig. 4. Dependence of the EUV emission in the water window from the liquid nitrogen jet on the laser polarization with respect to the axis of the liquid jet, at otherwise identical conditions, i.e., 250 ps pulse duration and 50 mJ pulse energy. The two spectra with parallel polarization were taken directly before and after the spectrum with perpendicular orientation (*upper curve*)

2 Results

The visual appearance of these experiments with ultrashort intense laser pulses interacting with the continuous liquid jet target is a very bright, white light spot at the laser impact position. We observed suddenly occurring fluctuations in this light emission even though the jet seemed to be flowing steadily on a macroscopic scale. We attribute these fluctuations to microscopic changes of the jet pointing direction. This view is supported by the known sensitivity of small laminar jets to external perturbations such as the impact of the intense laser pulse 5 mm away from the jet nozzle [6]. The local heating will cause a shock wave, which can reach the nozzle within 15 µs, assuming a sound velocity of 320 m/s for liquid Ar in the jet [15]. This is far later than the end of one laser event including decay of metastable states, emission of ions and expansion of the localized plasma, but sufficiently early that the jet can establish a new position prior to the subsequent laser pulse. We observed further that the jet moved in several such "steps" in one direction which could be compensated for by moving the focusing lens a few tens of micrometers for every step. These sensitive jumps were most frequent for the shortest laser pulse duration and scarcely observed at 250 ps.

2.1 Soft X-ray and EUV spectra

In Figs. 2 and 3 the liquid jet plasma emission in the wavelength region of the water window is shown for the two target materials, liquid nitrogen and liquid argon, respectively. For nitrogen the emission lines are easily identified as being due to hydrogen-like and helium-like ions. Since the nitrogen spectra show no further details above 3.4 nm, the presented graphs focus on shorter wavelengths. Although the identification of the lines is more difficult in the case of argon, we can unambiguously identify Ar^{8+} in the plasma. Other intense peaks can be assigned to carbon-like ions (i.e., Ar^{12+}, see below) and possibly even higher charge states.

For both target materials we observe a strong dependence of the EUV flux on the laser pulse duration, leading to the strongest emission in the case of nitrogen for a 250 ps pulse duration and to an intensity maximum for ≈ 1 ps pulses in the case of argon. The highest flux in a single line is obtained for nitrogen in the Ly-α line at 2.48 nm at 50 mJ pulse energy, being 1.2×10^{11} photons pulse^{-1} sr^{-1}; in comparison, a flux of 8.7×10^{10} photons pulse^{-1} sr^{-1} was found in the He-α line at 2.88 nm at 50 mJ pulse energy. The emission in the Ly-α line corresponds thus to a conversion efficiency of 0.3%. Table 1 shows the dependence of the measured conversion efficiencies on the laser pulse duration for the two prominent nitrogen lines, assuming isotropic emission in 4π. However, the total emission of 6.2×10^{11} photons pulse^{-1} sr^{-1} (710 fs, 30 mJ) in the wavelength interval between 2.0 and 4.0 nm is two times higher for argon than for nitrogen (3.6×10^{11} photons pulse^{-1} sr^{-1}, 250 ps, 50 mJ). For argon the maximum emission is observed around 3 nm. Note that for the shortest pulse duration of 70 fs the maximum emission is found at energies lower ($\lambda_{max} \approx 3.1$ nm, see Fig. 3a) than for longer pulses around 1 ps ($\lambda_{max} \approx 2.8$ nm, see Fig. 3b), in spite of the higher intensity in the case of ultrashort pulses.

From the nitrogen spectra shown one might get the impression that a shift of the distinguishable series limit is found with respect to the laser pulse duration. Due to the limited signal-to-noise ratio, a quantitative analysis of this effect in order to calculate the electron density of the plasma was not carried out. For the same reason the observable rise of the satellite lines for a shorter pulse length is not the subject of further investigation. A possible nitrogen K_α emission at 392.4 eV corresponding to 3.16 nm was not strong enough to be identified clearly.

The dependence of the EUV emission on different laser polarizations with respect to the liquid jet axis was studied with nitrogen as the target material. Figure 4 shows spectra each of which is averaged over 2400 pulses with 50 mJ pulse energy at 250 ps. The measurements were performed carefully within several minutes to ensure identical conditions for stable plasma formation, apart from the change in polarization. For laser polarization perpendicular to the jet, the measured photon number in the Ly-α line (1.2×10^{11} photons pulse^{-1} sr^{-1}) is about 30% higher than for parallel polarization (7.3×10^{10} photons pulse^{-1} sr^{-1}). The emission in the He-α line (8.9×10^{10} versus 6.6×10^{10} photons pulse^{-1} sr^{-1}) shows the same characteristics. The relative accuracy of this data is about 10%. However, for shorter pulse durations this dependence on the orientation of the laser polarization could not be found. We note that due to the less stable jet operation it was not possible to verify the advantage of the perpendicular polarization at shorter pulse lengths.

While most of our observations focused on the water window we also studied the EUV emission of argon at longer wavelengths between 13 nm and 20 nm and found a similar dependence on the pulse duration. Since there is no calibration data available for the grating in this wavelength range, the calculation of absolute photon numbers is based on theoretical data obtained by [13]. The data shown (Fig. 5) represent a lower limit of absolute photon numbers due to the fact that the theoretical data overestimates the actual grating efficiency. The trace showing higher intensity was obtained for 250 ps and 50 mJ per pulse without a filter in front of the grating. The less-intense trace was recorded at 2 ps and 30 mJ using a Zr filter on a Si substrate. We observed an integrated photon flux of 4.0×10^{11} photons pulse^{-1} sr^{-1} at 250 ps pulse duration in the wavelength range 14–18 nm, comparable to the measured flux in the water window. Due to both uncertainties in the filter thickness and the use of theoretical efficiency data, these absolute photon numbers are estimated to be accurate within a factor of 2, only.

The line assignments in Figs. 2 to 5 are based on the atomic data compiled by Kelly [16]. While for nitrogen the assignment of the lines is readily performed (see above), a complete assignment is not possible for the argon data at present, since the resolution of the spectrograph is insufficient in view of the numerous possible transitions ($\lambda/\Delta\lambda \approx 100$ at

Table 1. Measured X-ray fluxes for nitrogen lines (photons pulse^{-1} sr^{-1}) and their corresponding conversion efficiencies η (%) at given laser pulse energies (E_L; mJ) and intensities (I; W cm^{-2})

τ	250 ps	2.25 ps	70 fs
E_L	50	25	25
I	1.3×10^{13}	9.8×10^{14}	3.0×10^{16}
He-α	8.7×10^{10}	3.4×10^{9}	3.0×10^{8}
Ly-α	1.2×10^{11}	3.5×10^{9}	1.7×10^{8}
$\eta_{He-\alpha}$	1.5×10^{-1}	1.1×10^{-2}	1.2×10^{-3}
$\eta_{Ly-\alpha}$	2.5×10^{-1}	1.3×10^{-2}	8.0×10^{-4}

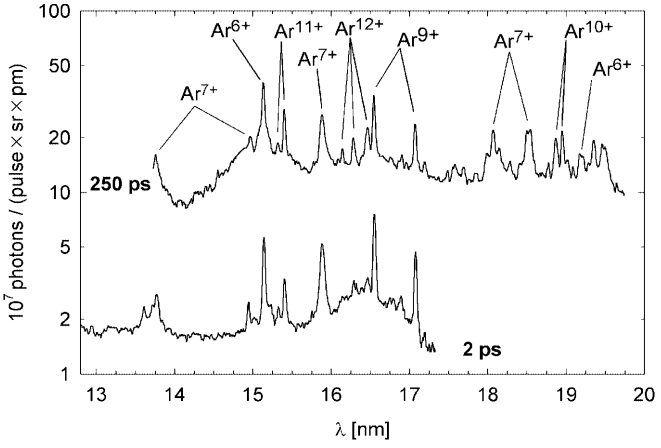

Fig. 5. EUV emission from the liquid argon jet at longer wavelengths. The upper trace was recorded without a filter at 250 ps pulse duration (50 mJ). The less-intense trace was recorded at 2 ps (30 mJ) and a SiZr filter (200 nm each). Emission lines of argon ions with charge states of up to 12+ are found

2.4 nm). The clearly identified doublet lines at 4.87 nm and 4.91 nm of the Ar^{8+} ($2p^6 \leftarrow 2p^5\,3s$) transition from the singlet and triplet fine structure levels are used for the absolute wavelengths calibration of the spectrograph for the shorter wavelengths. As is seen from Fig. 3, the identification of the lines towards shorter wavelengths down to 3 nm is partly possible and allows for claiming presence of at least Ar^{12+} in the laser-generated plasma. At wavelengths below 3 nm, the increasing line density makes a line assignment even more difficult. Moreover, around 2 nm we find lines which are not listed yet in [16]. Surprisingly, the spectra between 13 and 20 nm show emission lines from argon ions with charge states of up to Ar^{12+} as well, but the EUV emission can be attributed mainly to ions with lower charges between Ar^{6+} and Ar^{9+}.

2.2 Ionic debris

The kinetic energy distributions of the ionic debris emitted from the laser-generated plasma from both argon and nitrogen jets are depicted in Fig. 6, which shows kinetic energies that exceed 100 keV for nitrogen and even 200 keV for argon. The maximal kinetic energy was found to depend on the laser pulse duration, as did the EUV emission discussed above. For nitrogen the highest energies were obtained at a pulse duration of 2.25 ps. Although a complete data set is not available for argon, the existing data indicates a similar qualitative behavior for the energy distributions but with higher resulting energies (see Fig. 6). This may be attributed to the higher charge states and thus stronger Coulomb repulsion in the argon plasma.

Figure 7 shows a sequence of ionic distributions taken while moving the focusing lens in steps of 10 μm sideways. This results in scanning the laser focal spot perpendicularly to the liquid jet. Each of the five smooth curves is an average over some fifty laser shots at 5 different focal spot positions. The additional presentation of a single shot spectrum, which shows the most energetic energy distribution, illustrates the large variations of the ion energy spectra for individual shots. As one would intuitively expect, the highest ionic energies are observed while hitting the center of the jet. Moving the focal spot 40 μm sideways away from the jet results in a kinetic

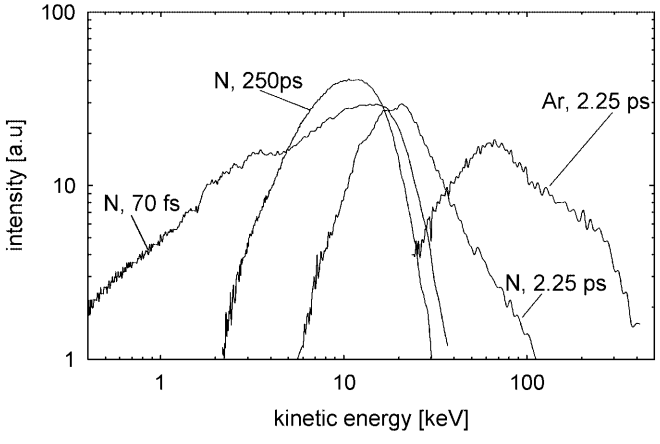

Fig. 6. Kinetic energy distribution of the nitrogen and argon ions as obtained from individual laser shots. The highest kinetic energies exceed 100 keV and 200 keV measured at a pulse duration of 2.25 ps for nitrogen and argon, respectively

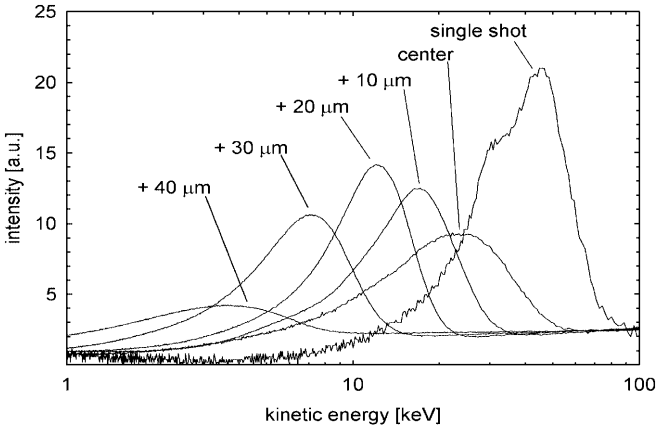

Fig. 7. Kinetic energy distribution of the argon ions for different positions of the laser focal spot with respect to the jet. The incremental change in transversal position is 10 μm

energy lowered by one order of magnitude. The fact that the kinetic energy is not lowered to zero is due to residual laser intensity ($\approx 10\%$ of I_{max}) and the continuous gas evaporation from the jet as a result of the inherently high vapor pressure of cryogenic liquids (see above).

This emission of highly energetic ions is a severe issue because of potential damage induced by debris from the target material. This becomes evident by looking at Fig. 8, which shows an electron micrograph of the platinum nozzle used for jet formation. The outer surface of the nozzle shows strong degradation after 10 h of jet operation at a laser repetition rate of 20 Hz (i.e., 7.2×10^5 shots). The initially round nozzle hole of 20 μm diameter still partly visible in the center is now surrounded by a conical crater of 60 μm diameter and 30 μm depth, which corresponds to a removal of about 3×10^4 μm^3 of material. The large conical crater is decorated with numerous small damage regions of about 1 μm width and 0.1 μm depth. An interpretation of the formation of the smaller craters by single ion bombardment directly from the plasma can be excluded for two reasons. First, the formation

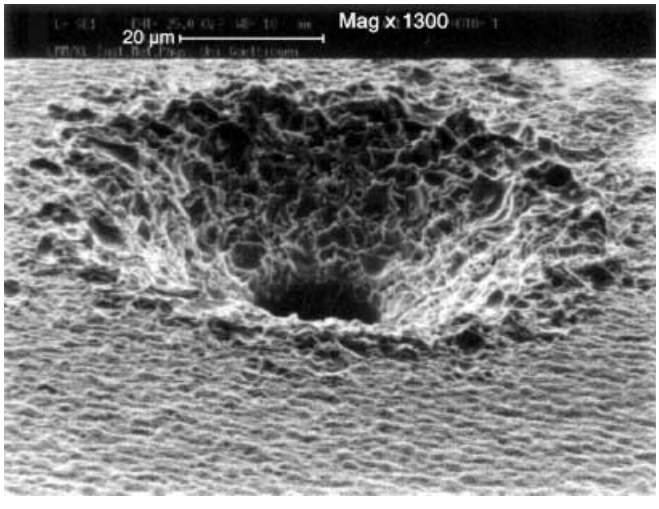

Fig. 8. Micrograph of the nozzle orifice after its use as a liquid jet source. The width of the conical crater reaches four times the initial diameter, which was 20 μm (still visible in the center); the depth of the cone exceeds 20 μm

of a μm-sized crater by an individual ion would require an impact energy of several hundred MeV, i.e., energies exceeding by several orders of magnitude the observed maximum energy of individual ions. Thus, it would require an unlikely cooperative action of several thousand ions. Secondly, at the high density in the steam blanket surrounding the jet, fast ions cannot reach the nozzle close to the liquid jet axis. Therefore, the erosion should increase with increasing distance from the nozzle center. This is the exact opposite of the observation. Furthermore, it is known for laser-generated plasmas from solid targets that the ionic emission is highly anisotropic, peaking strongly for an emission direction perpendicular to the surface [17].

Based on these arguments, we suggest a model explaining the nozzle erosion as a consequence of a secondary arc discharge occurring between the plasma in the focal spot and the grounded nozzle. The quickly parting electrons leave behind a transiently charged plasma spot. The curved surface of the plasma target modifies strongly the plasma expansion behavior and leads to a longer lasting separation of the electrons and ions compared to the planar case [18]. Therefore, a high positive charge can be build up in the plasma region such that its potential is sufficiently high to ignite a gas discharge. This ignition is facilitated by the pre-ionization of the surrounding steam blanket due to the high EUV photon flux from the plasma. The increasing gas density towards the interior of the gas cloud will lead to stronger discharge currents and consequently to a higher sputtering rate closer to the jet axis. The much higher vapor pressure of argon together with its superior sputter efficiency compared to nitrogen explains why the nozzle is far less corroded in experiments involving nitrogen. Rough estimates of several parameters such as focal spot size, electron versus ion conductivity in an argon plasma, capacity, etc. [19], lead to a consistent picture with the observed quantity of removed material in the case of the argon jet and the almost absence of sputtering for the nitrogen jet. In addition, during the interaction of the laser with the liquid argon jet we observed green and blue light emission from the surface of the jet nozzle, possibly caused by highly energetic ion impact. All these mentioned observations should be considered when sensitive optical components are to be placed close to such a EUV light source for applications such as, for example, lithography.

3 Discussion

3.1 Soft X-ray and EUV spectra

Liquid nitrogen jets have already been irradiated with nanosecond [10] and picosecond [6] lasers. In [6] a flux of 4.5×10^{11} photons pulse^{-1} sr^{-1} was obtained in the 2.88 nm line, using a 100 ps, 70 mJ laser at a wavelength of 532 nm with a 3 mJ prepulse at 366 nm. This corresponds to a conversion efficiency of $\eta = 0.5\%$. The delay between the pre- and the main pulse was several ns [20]; the diameter of the liquid jet was 5 μm. In the present work with the laser parameters being 250 ps pulses with 50 mJ at 800 nm, we measured conversion efficiencies of $\eta = 0.3\%$ and $\eta = 0.1\%$ for the Ly-α and He-α lines, respectively (see above). Besides the shorter wavelength of the laser used in [6], the double pulse scheme, in which the first pulse serves as the igniter of the plasma expansion and the second provides the main source of energy to heat the preformed plasma, is one probable reason for the higher efficiency obtained. More recent experiments performed in Göttingen [10] with a commercially available frequency-doubled Nd:YAG laser (532 nm) employed a single 3 ns laser pulse of 250 mJ on a 30 μm diameter jet. In this case 1.5×10^{12} photons pulse^{-1} sr^{-1} in the Ly-α line ($\eta = 0.7\%$) versus 7×10^{11} photons pulse^{-1} sr^{-1} in the He-α line ($\eta = 0.3\%$) were observed. Here the higher conversion efficiency may be attributed to the much longer laser pulse and higher pulse energy. Since our experimental conditions were different from those described in [6, 10], a more accurate comparison of the efficiencies is difficult. Therefore, one needs a better understanding of the involved mechanisms.

For a comparison of the emitted photon flux observed in the present work for the two different target materials, either the total flux or the spectral brilliance can serve as the criterion. Although the total emission in the water window is higher for argon than for nitrogen, the brilliance in a restricted energy interval (i.e., $\Delta\lambda = 0.1$ nm) can be much higher for nitrogen due to the fewer remaining electrons with correspondingly less available transitions. In contrast, the emission in the case of argon is distributed in numerous lines, thus leading to a reduced spectral brilliance. This demonstrates the two counteracting effects of the atomic number Z on the spectral brightness which have to be taken into account while optimizing a potential EUV light source. A target material with emission in a narrow wavelength interval only, may reduce the need for narrow band filtering, which could reduce the light intensity by one or two orders of magnitude. Notably, typical multilayer mirrors frequently used in this energy domain are highly reflective only for the narrow wavelengths band for which the mirror was optimized. This reflectivity decreases rapidly for wavelengths outside the multilayer bandwidth, typically of $\lambda/\Delta\lambda \approx 100$ at $\lambda = 13$ nm.

It is furthermore instructive to compare our EUV spectra from the liquid jet plasma to those obtained from free rare gas clusters by other groups [21, 22]. In [21] EUV spectra from argon cluster plasmas generated with a comparable laser system (20 mJ, 350 fs, $\approx 8 \times 10^{17}$ W cm^{-2}) are given. Although the reported spectra between 3 and 18 nm show similarities to our measurements, the obtained photon flux from the liquid jet plasma is higher than that reported for the cluster target, and there are no argon ions found in the cluster plasma with charge states higher than 10+. However, in [23], where a 0.5 J Nd:YAG laser, with 0.9 ns pulse duration resulting in moderate intensities of 10^{14} W cm^{-2}, was used to irradiate gas puffs of different gases, argon spectra in the water window were reported with emission lines from argon ions with charge states of up to 13+. Moreover, the reported flux is higher by about a factor of 2. In [22], where a 130 fs laser (500 mJ, $\approx 1.5 \times 10^{16}$ W cm^{-2}) was used to irradiate argon clusters ($\varrho \approx 5 \times 10^{18}$ cm^{-3}), the emission between 2 and 6 nm is attributed exclusively to Ar^{8+}. The authors found 4 broad emission bands from the $nd \rightarrow 2p$ ($n = 5, 4, 3$) series and the $3s \rightarrow 2p$ series. The emission maximum observed is at a wavelength of ≈ 5.2 nm or even longer, while in our spectra the maximum is found near 3 nm. Moreover our better resolved spectra with typically 5 eV resolution show the presence of emission lines down to 1.5 nm. Since the series of Ar^{8+} terminates around 3 nm, there is a need for another explanation of the origin of these lines. Either a series of increasing charge

states of up to Ar^{14+} or, alternatively, a superposition of series from lower charged ions (e.g., $Ar^{8+\cdots 10+}$) but with a population in higher excited states, as was proposed by Ditmire and coworkers, can provide tentative explanations for these spectral features. Note that Ar^{8+} is Ne-like and thus forms an energetically favorable electronic configuration. This could explain why in [22] mostly this ion and lower charges were visible. In our liquid jet plasma the next lower shell ($2p$) also was excited or ionized and immediately many more states become visible.

From the results described in Sect. 2 and the given references, we can state that it is not mainly the highest laser intensity that leads to the most efficient generation of EUV radiation but the longer duration of the laser pulse in relation to the pulse energy. In agreement with this are cluster target experiments recently reported where it was shown that the pulse length dependence of the absorption process maximizes the efficiency at a pulse duration of about 1 ps [24, 25]. This is close to the pulse durations around 1 ps that lead to the highest emission in the water window region for the liquid rare gas jet of argon. However, for the liquid nitrogen jet the strongest emission was found clearly at a pulse duration of 250 ps. For single pulse operation without a prepulse the present data establish the lower limit for the optimal pulse duration for maximum EUV emission of laser-generated micro-plasmas from a liquid jet target.

3.2 Nozzle erosion

The nozzle system to create thin liquid jets in vacuum is one of the most important features of our laser-driven EUV source. Stable jet formation over long periods and at high laser frequencies strongly depends on the operation conditions of the nozzle. Consequently the observed degradation of the nozzle after only a few hours of operation requires closer investigation. Experiments in generating liquid argon jets with no laser–jet interaction result in far less corroded nozzles, which indicates the role of the produced argon ions in regard to erosion. Other nozzle systems, e.g., glass capillaries, have been used successfully to produce thin liquid jets at room temperature [26] and may be used for cryogenic liquid jets as well. The different nozzle geometry and material give rise to the assumption that this kind of nozzle will not be affected in the manner observed.

We find that the nozzle system presented in this paper is not suited for high laser repetition rates due to the observed microscopic instabilities [10]. Since repetition rates in the kHz range are necessary for the high average EUV power needed for lithography, other nozzle systems have to be examined for this purpose.

4 Conclusion

Detailed EUV spectra emitted from laser-generated argon and nitrogen plasmas formed on liquid jets were reported. We found that the EUV emission strongly depends on the laser pulse duration and was a maximum under our experimental conditions for pulse durations of 250 ps and ≈ 1 ps for nitrogen and argon, respectively. The emission in the water window was attributed to hydrogen- and helium-like nitrogen and, in the case of argon, to ions with charge states of up to 13+.

Similar to the EUV emission, the observed ionic debris from the laser-generated plasmas showed a pulse-length dependence as well. Less energetic ions were emitted at the longest and shortest pulse durations, as compared to pulses of around 1 ps, where ion energies of up to some hundred keV were measured.

Acknowledgements. The authors thank E. Caprin and M. Bougeard for technical assistance with the vacuum system, as well as M. Perdrix, P. Meynadier and O. Gobert for perfect operation of the femtosecond laser system. G. Schmahl is thanked for his support as well as S. Rehbein for the fabrication of the grating. Ch. Ellert gratefully acknowledges a Marie-Curie grant of the European Community. This work has been funded partially by the DFG under contract number Sch/1118/4-1.

References

1. J. Thieme, G. Schmahl, D. Rudolph, E. Umbach: *X-Ray Microscopy and Spectromicroscopy* (Springer-Verlag, Berlin 1998)
2. J.P.H. Benschop, A.J.J. van Dijsseldonk, W.M. Kaiser, D.C. Ockwell: Solid State Technol. **42**(9), 43 (1999)
3. T.W. Johnston, J.M. Dawson: Phys. Fluids **16**, 722 (1973); D. Giuletti, L.A. Gizzi: Riv. Nuovo Cim. **21**(10), Sect. 3.1 (1998)
4. A. McPherson, T.S. Luk, B.D. Thompson, A.B. Borisov, O.B. Shiryaev, X. Chen, U. Boyer, C.K. Rhodes: Phys. Rev. Lett. **72**, 1810 (1994)
5. A. McPherson, B.D. Thomson, A.B. Borisov, K. Boyer, C.K. Rhodes: Nature **370**, 631 (1994)
6. M. Berglund, L. Rymell, H.M. Hertz, T. Wilhein: Rev. Sci. Instrum. **69**, 2361 (1998)
7. H. Hora: *Plasmas at High Temperature and Density*, Chapt. 11.2 (Springer-Verlag, Berlin 1991)
8. F. Brunel: Phys. Rev. Lett. **59**, 52 (1987)
9. P. Gibbon, A.R. Bell: Phys. Rev. Lett. **68**, 1535 (1992)
10. M. Wieland: Diploma thesis 1999, and unpublished results
11. http://www-drecam.cea.fr/spam/reseaulaser/luca/luca1.htm
12. T. Wilhein, S. Rehbein, D. Hambach, M. Berglund, L. Rymell, H.M. Hertz: Rev. Sci. Instrum. **70**, 1694 (1999)
13. http://www-cxro.lbl.gov/optical_constants/
14. T. Wilhein, D. Rothweiler, A. Tusche, F. Scholze, W. Meyer-Ilse: In *X-ray Microscopy IV*, ed. by V.V. Aristov, A.I. Erko (Bogorodskii Pechatnik Publishers, Chernogolovka 1994) p. 470
15. http://www.webelements.com
16. http://cfa-www.harvard.edu/amdata/ampdata/kelly/kelly.html
17. S. Bollanti, R. Cotton, P. Di Lazarro, F. Flora, T. Letardi, N. Lisi, D. Batani, A. Conti, A. Mauri, L. Palladino, A. Reale, M. Belli, F. Ianzini, A. Scafati, L. Reale, M.A. Tabocchini, F. Albertano, A.Ya. Faenov, T. Pikuz, A. Oesterheld: Il Nouvo Cim. **18D**, 1241 (1996)
18. G. Manfredi, S. Mola, M.R. Feix: Phys. Fluids B **5**, 388 (1993)
19. M. Faubel: unpublished results
20. M. Berglund, L. Rymell, H.M. Hertz: Appl. Phys. Lett. **69**, 1683 (1996)
21. E. Miura, H. Honda, K. Katsura, E. Takahashi, K. Kondo: Appl. Phys. B **70**, 783 (2000)
22. T. Ditmire, T. Donelly, A.M. Rubenchik, R.W. Falcone, M.D. Perry: Phys. Rev. A **53**, 3379 (1996)
23. H. Fiedorowicz, A. Bartnik, M. Szczurek, H. Daido, N. Sakaya, V. Kmetik, Y. Kato, M. Suzuki, M. Matsumura, J. Tajima, T. Nakayama, T. Wilhein: Opt. Commun. **163**, 103 (1999)
24. J. Zweiback, T. Ditmire, M.D. Perry: Phys. Rev. A **59**, R3166 (1999)
25. L. Köller, M. Schumacher, J. Köhn, S. Teuber, J. Tiggesbäumker, K.H. Meiwes-Broer: Phys. Rev. Lett. **82**, 3783 (1999)
26. H.M. Hertz, L. Rymell, M. Berglund, L. Malmqvist: Proc. SPIE **88**, 2523 (1995)